Chapter 2
Moisture and Heat

Under a cold climate, water exists in solid, liquid and gaseous states at, above and below the surface. Water can undergo change of state on time scales that vary from hours to days and seasons, to multi-year periods. Phase change involves energy and thus energy balance plays a major role in the detention or the release of water to runoff and river flow. Hinzman et al. (1991) stated that the thermal and moisture regimes are closely related to each other and to the characteristics of the active layer and therefore have a marked influence on permafrost dynamics. This chapter reviews briefly the fundamentals of moisture and heat fluxes at the atmospheric boundary layer and below-ground.

2.1 Precipitation

Water vapor in the atmosphere can be (1) advected into a permafrost region through planetary circulation, with synoptic scale disturbances (at horizontal length scale of ~10^3 km) and from nearby sources; and (2) recycled within the same region by evaporation and precipitation (Serreze and Barry 2005).

2.1.1 General Pattern

- Low temperatures in permafrost regions limit the amount of moisture in the atmosphere. Between 70° N and the North Pole, the precipitable water (which is depth of water obtained if all moisture in the atmospheric column is condensed) is about 2.5 mm in January and 24 mm in July (Serreze and Barry 2005). Most land areas north of 70° N are considered to be a polar desert (Bovis and Barry 1974). Moisture, hence precipitation, increases southward.
- Antarctica has a ring of high precipitation on the coastal permafrost areas that surrounds the central desert area with <50 mm year^{-1} of snow accumulation

DOI 10.1007/978-3-642-23462-0_2,

Fig. 2.1 Under strong oceanic influence, a belt of high precipitation and frequent cloudiness surrounds the Antarctic continent, as indicated by the clouds and summer snow that cover the rugged lands and glaciers at Lockroy, Antarctic Peninsula, February 2011

(Connolley and Cattle 1994). Under a strong oceanic influence, snow, rain and frequent cloudiness are common in the Antarctic Peninsula (Fig. 2.1).

- In alpine permafrost regions, elevation and topographic orientation significantly affect precipitation distribution. On the Tibetan Plateau, for example, moisture-bearing airflow comes from the southeast monsoon and there is a tendency for annual precipitation to decline northward and westward, with orographic influence increasing the precipitation at high elevations. Annual precipitation of the Tibetan Plateau drops from about 4,000 mm in the southeast to under 100 mm in the north (Zhou et al. 2000).
- Moist onshore winds, in concert with high and steep topography, create high precipitation zones (e.g. the Svalbard Islands and eastern Baffin Island). Sea ice restricts moisture flux from the ocean to the atmosphere and winds blowing from the ice-covered sea to the land do not yield high precipitation unless there are polynyas (open water surrounded by sea ice) nearby.

2.1.2 Cyclones

- The average position of a frontal belt may have long-term environmental implications. The mean summer position of the arctic front coincides with the northern edge of the Canadian boreal forest, or the treeline (Bryson 1966). Derksen et al. (2008) also found a band of heavy snow accumulation running

roughly along the treeline and suggested its correspondence with the preferred zone of front development.

- During the northern winter, low precipitation is experienced in those permafrost areas under the influence of high pressure, including Siberia, the Mackenzie District and its adjacent areas to the east and the Canadian Archipelago other than eastern Baffin Island. On the other hand, synoptic-scale eddies associated with planetary wave (created by colossal meander of high altitude air stream) transport much vapor. Frequent cyclonic activities occur in the Baffin Bay area and from Iceland extending northeastward to the Barents Sea, with incursions into northwestern Eurasia (Serreze and Barry 2005), carrying substantial vapor to sub-polar permafrost areas and depositing precipitation along their tracks. In summer, North Atlantic cyclonic activity diminishes but cyclones persist in the Baffin Bay area and increase in the central Arctic Ocean and in Siberia.
  Around Antarctica, the coastal fringes and the Antarctic Peninsula have high frequencies of cyclones all year round except at certain locations such as the Bellingshausen Sea (Simmonds et al. 2003). These high latitude cyclones are especially common in winter. They travel with an eastward component due to the coriolis effect, and spiral towards the continent, bringing heat and moisture to the permafrost areas along the continental margin. However, the storms do not penetrate deep into the interior, which is often under high pressure and has arid conditions.
- On a local level, cyclogenesis (development or strengthening of cyclonic circulation) enhances moisture transport. For example, the margins of polynyas favor the formation of winter cyclones. During the open water season in late June to mid-October, heat and moisture fluxes from southern Beaufort Sea also contribute to cyclogenesis, sending storms to northern Mackenzie Basin (Hudak and Young 2002). High mountain ranges block the path of onshore wind. Cyclones decay on the upwind side but lee cyclones can form downwind of the large-scale mountain. The Western Cordillera, for example, often blocks or modifies the passage of cyclones from the Pacific but lee cyclogenesis is common east of the Rockies (Szeto et al. 2008b). In South America, cyclones are weakened on the western flank of the Andes and the Antarctic Peninsula but they regenerate on the lee-side of the mountains (Hoskins and Hodges 2005).

2.1.3 Recycling

Local convection recycles moisture and deposits precipitation, mainly in the summer. Convectional summer precipitation tends to be variable in space and exhibits pronounced inter-annual variability. Figure 2.2 shows convectional rainfall on the Tibetan Plateau and in the Mackenzie River Basin near Yellowknife. For large basins where mountain slopes are heated more strongly than the flatlands, a regional mountain-plains circulation (e.g. the advection of moisture in the Mackenzie basin from the Interior Plains to the Cordilleran foothills)

Fig. 2.2 Recycling of moisture during the summer giving rise to convectional precipitation: (**a**) hail storm at Yanshiping on the Tibetan Plateau, July 1986, and (**b**) rainfall near Yellowknife in Mackenzie Basin, July 1989

enhances precipitation over the mountain zones. On the other hand, for the Lena basin that lacks the mountain-plains circulation mechanism, evaporation and recycling regulate precipitation variability within the basin. The recycling ratio (fraction of total precipitation derived from local evaporation) is about 25% for both basins (Szeto et al. 2008a).

2.1.4 Trace Precipitation

Trace precipitation is the amount of precipitation so low (under 0.2 mm) that it cannot be measured by conventional types of precipitation gages. Woo and Steer (1979) experimentally obtained an estimate of its average intensity to be 0.01 mm h^{-1}. Its frequent occurrence at some locations makes it a significant contributor of moisture. In the dry summer of 1977, the polar desert site of Resolute received an estimated 1.53 mm of trace rainfall, representing 17% of the total rainfall recorded by the weather station. These results reinforce the postulation by Brown et al. (1968) that without considering trace precipitation, the recorded amount for 1964 at Barrow, Alaska, could be as little as two-thirds of the actual.

Trace precipitation in permafrost regions can have several origins.

1. The flow of warm air over cold air promotes ice fogs in the winter. An example is the Mackenzie River Basin that lies downwind of the Pacific air flow. The descending air warms up after crossing the Western Cordillera and rides on the more stagnant cold air layer on the Interior Plains, giving rise to temperature inversion that favors ice fog development. Similarly, the passage of warm air over radiatively cooled valleys is conducive to ice fog formation, as is common in Fairbanks during winter (Benson 1970).
2. Clouds are a source of trace precipitation. Cloudiness frequently prevails in areas with alpine permafrost, as well as in maritime locations at high latitudes where low stratus represents a common cloud form.
3. On a local level, coastal fogs are common in the fall when open water near coastal areas or polynyas produces warm moisture-laden air that advects and

Fig. 2.3 Coastal fog drifting over cold land surface in Resolute, Cornwallis Island, in late August when bays and inlets were ice-free and ground freeze already started on land

condenses over cold sea ice and its adjacent lands (Fig. 2.3). A melting snow cover can similarly provide moisture to the atmosphere that condenses as trace precipitation (Barry and Hare 1974).

2.2 Surface Energy Balance

The net radiation at the surface (Q^*) is the radiation balance from net short-wave (K^*) and net long-wave (L^*) components

$$Q^* = K^* + L^* \tag{2.1}$$

with all units in J s^{-1} m^{-2} (or W m^{-2}). Solar irradiance represents the energy delivered by the sun to a surface. At the top of the atmosphere and perpendicular to the incoming solar radiation the magnitude is about 1,360 W m^{-2} (known as the solar constant, but it has slight variations, for instance during the sunspot cycle) and some of this radiation is absorbed, scattered or reflected as it enters the atmosphere. Since most permafrost areas are located at high latitudes, solar radiation meets the surface at low angles and therefore the amount received becomes progressively less towards the poles. During the winter, solar radiation input becomes negligible or nil as the polar region experiences perpetual or long nights. On the other hand, long summer days increase the duration of solar radiation input (Fig. 2.4) so that over a

Fig. 2.4 Eidsbotn Fiord, Devon Island, at 76° N under mid-night sun in June 1979. In high latitudes, long daylight hours augment solar radiation input to the daily total even though the sun is at low angles during the early hours

24-h period, the amount received can be comparable to that of more temperate areas. Using data from two stations in Canada, Fig. 2.5 shows the northward reduction in solar radiation and its strong seasonal asymmetry.

Part of the short-wave radiation reaching the surface is reflected. The albedo α is

$$\alpha = K\uparrow / K\downarrow \tag{2.2}$$

and

$$K^* = (1 - \alpha)K\downarrow \tag{2.3}$$

with the arrows indicating the upward or downward directions of short-wave radiation K. In cold regions, an extensive presence of snow and ice with a high albedo reflects much of the incoming short-wave radiation. Prolonged snow and ice cover during each year greatly reduces the net amount of short-wave receipt in permafrost areas.

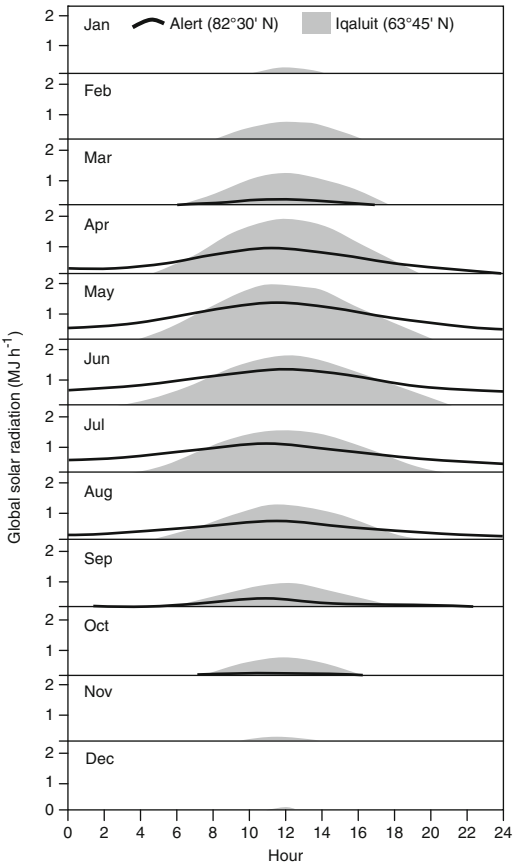

Fig. 2.5 Mean hourly global solar (incoming short-wave) radiation at two Canadian stations, located at Iqaluit (63°45′N) and at Alert (82°30′N), showing poleward reduction in solar radiation and strong seasonal asymmetry, with long daylight hours increasing the daily total in the summer and prolonged period of winter darkness yielding little or no solar radiation

The amount of long-wave emission depends on the temperature of the emitting body such that

$$L = \varepsilon \sigma T^4 \tag{2.4}$$

with T being the temperature (in K), σ the Stefan-Boltzman constant ($= 5.67 \times 10^{-8}$ W m^{-2} K^{-4}) and ε being emissivity, which is between 0 and 1. L^* is the balance between incoming ($L\downarrow$) and outgoing long-wave radiation ($L\uparrow$). When the atmosphere is colder than the snow or ground surface, $L\uparrow > L\downarrow$. The reverse happens when the ground is colder than the air.

The net radiation energy at the surface is transferred to sensible heat (Q_H) that warms the air, latent heat (Q_E) for evaporation and ground heat (Q_G) to the soil

$$Q^* = Q_H + Q_E + Q_G \tag{2.5}$$

In summer, these terms are positive downward (i.e. towards the surface). All the terms can acquire a negative sign during part of the year when energy is lost instead of gained at the surface. The presence of a snow cover further modifies the partitioning of the energy balance, as will be shown in Chap. 4.

Heat flux into or out of the ground can be measured directly using a heat flux plate. Very often, it is calculated by the heat conduction equation

$$Q_G = K_T(dT_G/dz) \tag{2.6}$$

where K_T is thermal conductivity of the surface soil and dT_G/dz is temperature gradient at the ground surface (the top 0.02 m, say). The sensible and latent heat flux terms are elaborated below.

2.3 Evaporation

The latent heat flux is hydrologically important as it is responsible for sublimation of snow in winter and evaporation in summer. The terms evaporation and evapotranspiration have been used without clear distinction, and not only in hydrologic literature. From the atmospheric perspective, both represent an upward flux of vapor evaporated from the surface. The term evapotranspiration is much used to denote the combined processes of evaporation and transpiration losses to the atmosphere, and is applicable where there are vascular plants. For large tracts of permafrost areas, however, the ground is either barren or covered with non-transpiring lichens and mosses and the term evapotranspiration is inappropriate. In this book, the word evaporation will be used generically to denote vapor flux from the surface unless transpiration is clearly the dominant process.

Mendez et al. (1998) and Shutov et al. (2006) reviewed a number of methods that have been used to study evaporation in the permafrost environment. Here, four commonly used ones are described.

2.3.1 Eddy Fluctuation Method

Turbulence in the atmosphere gives rise to eddies that bring heat and moisture to and from the surface. Mass flux is the product of the vertical wind velocity (w), the density (ρ) and the magnitude or concentration of an entity (η) which can be momentum, temperature or humidity

$$Flux = \rho w \eta \tag{2.7}$$

The flux can be considered to comprise two components: a mean value and instantaneous fluctuations that deviate from the mean. Over time (such as 10 min to several hours, normally 0.5–1 h), the amounts of updraft and downdraft are equalized, at least theoretically assumed to be so. Then, the mean component would be zero. However, at any instant, there is a covariance between the deviation in the vertical wind flow (w') and departure of the entity from its long-term mean (η'). The product of these instantaneous deviations (i.e. $w'\eta'$), when averaged, is non-zero. Assuming that air density does not vary and turbulence is fully developed, the flux conveyed with the eddies is:

$$Flux = \rho \overline{w'\eta'} \tag{2.7a}$$

where the overbar denotes mean value.

Applied to latent heat flux,

$$Q_E = \lambda_v \rho_a \overline{w'q'} \tag{2.8}$$

and for sensible heat flux,

$$Q_H = C_a \rho_a \overline{w'T'} \tag{2.9}$$

with ρ_a and C_a being the density (kg m^{-3}) and heat capacity (J kg^{-1} K^{-1}) of air, λ_v being the latent heat of vaporization (2.5 GJ kg^{-1}). T', w′ and q' are instantaneous deviations of temperature (K), vertical wind speed (m s^{-1}) and specific humidity from their respective means. Specific humidity (q, dimensionless) is the ratio of mass of water vapor to the mass of moist air and it is related to vapor pressure (e in kg m^{-1} s^{-2}) through $q = 0.622\ e/PR$ with PR (in kg m^{-1} s^{-2}) being the atmospheric pressure. As they can be derived from one another, q and e will be used interchangeably in the following sections.

This method has the advantage of measuring the flux directly, but it has several requirements. (1) Highly sensitive sensors are needed to measure wind and humidity (or temperature for sensible heat flux). (2) Eddies tend to be smaller close to the surface and more intense measurements are required. (3) This method performs properly over relatively uniform terrain devoid of areas of preferred vertical motion, such that the mean vertical flow is zero or close to zero (Oke 1987). The last condition renders it impractical for steep slopes.

2.3.2 Aerodynamic Method

The aerodynamic method can be used to calculate latent and sensible heat fluxes. Using time-averaged profiles with measurements taken at two heights: z_2 at a higher level than z_1

$$Q_E = \rho_a \lambda_v D_E (u_2 - u_1)(q_2 - q_1) \tag{2.10}$$

$$Q_H = \rho_a C_a D_H (u_2 - u_1)(T_2 - T_1) \tag{2.11}$$

ρ_a, C_a and λ_v are as previously defined. T, q and u are time-averaged temperature, specific humidity and wind speed at two heights denoted by subscripts *2* and *1*. For most purposes, the drag coefficients (dimensionless), D_H and D_E, are assumed equal. Then

$$D_H = D_E = \kappa^2 [\ln(z_2/z_1)]^{-2} \tag{2.12}$$

Here, κ is the von Kármán constant, and the drag coefficient has to be adjusted for atmospheric stability (more detail presented in Sect. 4.3.2).

2.3.3 Bowen Ratio Method

The Bowen ratio method is based on energy balance and makes use of the ratio of the turbulent fluxes

$$B = Q_H / Q_E = (C_a \Delta T)/(\lambda_v \Delta q) \tag{2.13}$$

C_a and λ_v are as previously defined, ΔT and Δq are the differences in air temperature and specific humidity at two levels. B is known as the Bowen ratio. By assuming similarity of the turbulent exchange (or drag) coefficients for heat and vapor, this method has the advantage of not requiring wind measurements, but only air

temperature and humidity at two levels. In many difficult permafrost terrains, the Bowen ratio method is often a preference over the aerodynamic approach.

Combining the Bowen ratio and measured Q^* and Q_G, latent heat flux is obtained by

$$Q_E = (Q^* - Q_G)/(1 + B) \tag{2.14}$$

Note that low gradients for ΔT and Δq can cause significant error in B. In addition, Ohmura (1982) listed several criteria that should be satisfied when the Bowen ratio method is applied. It should not be used when $Q^* < 0$, when the latent heat flux is negative or during rain, and when Q_H and Q_E are of opposite signs.

2.3.4 Priestley and Taylor Method

Priestley and Taylor (1972) presented a method that requires easily obtainable data and is therefore well suited to remote permafrost locations. Equilibrium evaporation (Q_{eq}) has to be obtained first:

$$Q_{eq} = [s/(s + \gamma)](Q^* - Q_G) \tag{2.15}$$

Here, $\gamma \approx 0.66$ is the psychrometric constant (in kg m^{-1} s^{-2} C^{-1}), s is the slope of saturation vapor pressure-temperature curve, approximated by (Dilley 1968)

$$s = de_{sat}/dT = 35,473 \exp[17.269T/(T + 237.3)](T + 237.3)^{-2} \tag{2.16}$$

with e_{sat} being the saturated vapor pressure. s should be evaluated at the mean of the surface and air wet-bulb temperatures (Davies 1972), but since $s/(s + \gamma)$ is a slowly changing function of temperature, air temperature can be used as an approximation without incurring much error. The ratio of actual evaporation to equilibrium evaporation is α':

$$\alpha' = Q_E/Q_{eq} \tag{2.17}$$

and

$$Q_E = \alpha'[s/(s + \gamma)](Q^* - Q_G) \tag{2.18}$$

The information needed includes net radiation, temperature to obtain s, ground heat flux (measured with heat flux plates, or use Eq. 2.6) and a value for α'. Priestley and Taylor (1972) proposed that the best estimate of α' is its overall mean of 1.26. In permafrost areas, α' has been estimated using actual evaporation that is measured directly with lysimeters or obtained with the Bowen-ratio method (e.g. Boike et al. 2008).

Stewart and Rouse (1977) applied the Priestley and Taylor equation to two wet sites in northern Canada and substantiated the validity of $\alpha' = 1.26$ for summer evaporation from shallow lakes and sedge meadows. For a non-transpiring lichen heath which suppresses evaporation from the moist soils beneath, Rouse et al. (1977) obtained $\alpha' = 0.95$. Lichen woodland is a combination of transpiring spruce trees and a non-transpiring lichen mat and has $\alpha' = 1.13$, which is intermediate between a surface evaporating at the potential rate and that of the lichen heath. Clearly, evaporation is governed by energy supply but is restricted when moisture is limiting.

For non-vegetated gravel and loamy soil in the High Arctic, Marsh et al. (1981) obtained an empirical equation that relates α' to the soil moisture content

$$\alpha' = 1.26/[\exp(5.24 - 21.56\theta_w) + 1] \tag{2.19}$$

where θ_w is the volumetric soil moisture content at the top 0.10 m.

It is necessary to note that evaporation computed using the various equations presented is for a non-advective environment. Marsh and Bigras (1988) found that the Priestley and Taylor equation gives a good approximation of the evaporation from NRC Lake of moderate size (about 300 m by 200 m) in the continuous permafrost area of the Mackenzie River Delta (modeled total of 220 mm for 108 days of evaporation, compared with a total of 206 mm from water balance). However, for a small lake that varied in size from 0.01 to 0.006 km^2 between years, it yielded 342 mm year^{-1} of evaporation compared with 230 mm year^{-1} for the NRC Lake. The considerably larger evaporation loss from the small lake was attributed to heat advection. Advective heat flux has an influence on the Priestley and Taylor α'-coefficient. Bello and Smith (1990) obtained a summer seasonal estimate of $\alpha' = 1.35$ under local heat advection for a small tundra lake near Churchill, Manitoba. They also found that for individual days α' ranged from 1.0 to 2.0.

2.4 Energy Balance of the Active Layer

2.4.1 Energy Balance

As most hydrologic activities take place in the seasonal freeze-thaw zone, the focus here is on the energy balance of the active layer. Consider the thawing situation in a vertical column free of lateral heat gain or loss. The energy balance is

$$Q_G + Q_i = Q_s + Q_l + Q_{pf} \tag{2.20}$$

Here, the active layer gains energy from heat conducted from the surface (Q_G) and from rainwater or snowmelt that infiltrates the soil (Q_i). Note that water that does not directly penetrate the soil but is frozen on the ground surface will produce heat that is added to the conduction term. Energy is converted into sensible heat to

warm the active layer (Q_s), is consumed as latent heat for melting ground ice (Q_l), and is dissipated through conduction to the permafrost below (Q_{pf}).

Heat conduction into the active layer (Q_G) follows the temperature gradient, as indicated by Eq. 2.6. The presence of permafrost as a cold substrate throughout the thaw season ensures that a ground temperature gradient, directed downward, is maintained when the surface warms up. The gradient is enhanced when the thaw is shallow and the surface temperature is high.

Heat is conducted to the permafrost during the thaw season as the permafrost is colder than the active layer. Q_{pf} can be obtained with Eq. 2.6: use heat conductivity of the permafrost soil for K_T and use the temperature gradient at the permafrost table. It is further assumed that no water percolates into the permafrost and so no heat is convected into it.

The energy convected by the infiltrated water depends on the amount and temperature of the water infiltrated:

$$Q_i = C_w(T_w - T_s)\, dF/dt \tag{2.21}$$

with C_w being the volumetric heat capacity of water (J m^{-3} C^{-1}) that infiltrates at a rate of dF/dt (m s^{-1}). T_w and T_s are temperatures of the water and soil, respectively. Q_s can be calculated by

$$Q_s = C_T(dT_s/dt)Z \tag{2.22}$$

with C_T being the volumetric heat capacity of the soil and dT_s/dt being the daily temperature change over the active layer which has a thickness of Z.

The consumption of latent heat energy (Q_l) is dependent on the amount of ground ice at the thawing front

$$Q_l = \rho_i \lambda_f f_i (dh/dt) \tag{2.23}$$

for ρ_i being the density of ice, λ_f the latent heat of fusion, and f_i the ice fraction in the soil at the thawing front. dh/dt is the rate of ground thaw.

2.4.2 Thermal Conductivity and Heat Capacity

The bulk thermal conductivity (W m^{-1} C^{-1}) for a soil layer can be estimated when the fractions of mineral and organic materials, air, water and ice are known. One method for estimating thermal conductivity is (Farouki 1981):

1. For dry soil with a bulk density of ρ_b, the thermal conductivity K_{dry} can be estimated by

$$K_{dry} = (0.135\rho_b + 64.7)/(2700 - 0.947\rho_b) \tag{2.24a}$$

Table 2.1 Thermal conductivity and heat capacity of selected materials

Material	Thermal conductivity [W m^{-1} K^{-1}]	Volumetric heat capacity [J m^{-3} K^{-1} x 10^6]
Clastic material	2.93	1.92
Organic material	0.25	2.51
Air (10°C)	0.025	0.00125
Water (10°C)	0.57	4.18
Ice (0°C)	2.2	1.9
Snow: Fresh	0.06	0.2
Packed	0.70	0.8
Peat (80% pore space): Dry	0.06	0.58
Saturated	0.5	4.5
Icy	1.9	1.5
Clay (40% pore space): Dry	0.25	1.3
Saturated	1.6	3.0
Sand (40% pore space): Dry	0.3	1.25
Saturated	2.2	2.9

Source: de Vries (1963), Nicholson (1976), Oke (1987)

2. For wet soil

$$K_{sat} = \prod_{j=1}^{5} K_T(j)^{f(j)} \tag{2.24b}$$

with $K_T(j)$ and $f(j)$ being the thermal conductivity and volumetric fraction of the *jth* type of soil substance that includes mineral and organic materials, ice, water and air. The thermal conductivities of several typical materials are given in Table 2.1.

The thermal conductivity of frozen soil according to Johansen (1975; quoted by Farouki 1981) is

$$K_T(frozen) = (K_{sat} - K_{dry})(\theta_w/\varphi) + K_{dry} \tag{2.24c}$$

for θ_w being the volumetric fraction of soil moisture and φ being the soil porosity.

Following de Vries (1963), the heat capacity (J m^{-3} C^{-1}) can be calculated by

$$C_T = \sum_{j=1}^{5} C(j)^{f(j)} \tag{2.25}$$

Here, C_T is the bulk heat capacity and $C(j)$ is the heat capacity of the *jth* type of soil substance as previously defined.

Dividing thermal conductivity by heat capacity yields the thermal diffusivity (m^2 s^{-1})

$$D_T = K_T/C_T \tag{2.26}$$

The thermal properties vary with depth in the active layer and with time because of the intrinsic different between soil horizons and the seasonal changes in ice and moisture contents due to freeze-thaw and wetting-drying of the ground.

2.5 Ground Temperature

Ground temperature of permafrost necessarily requires winter freezing of the active layer and the constant presence of a below-freezing substrate. Of particular interest to permafrost hydrology is the heating and cooling of the active layer where hydrologic activities are concentrated.

- Fluctuations of temperature at all time scales, from daily to annual, are dampened with depth; the arrival of temperature peaks and troughs is also lagged progressively at depth.
- The presence of a snow cover reduces ground temperature response to air temperature variations and caps the surface temperature around 0°C during the snowmelt period.
- Soil materials, through their heat conduction and storage properties (which change with wet-dry and frozen-thawed conditions), give rise to substantial variations in temperature, sensible heat flux and ground thaw. Differences between the thermal regimes of organic and mineral soils are well documented (Nakano and Brown 1972; Yi et al. 2007) and the presence of an organic layer overlying mineral soil often produces a kink in the temperature profile.
- Freeze-back of the active layer undergoes the processes of heat conduction, active layer cooling and soil moisture freezing to form ground ice, all operating in directions opposite to ground thaw.
- The formation and melting of substantial ground ice at a certain depth in the soil column involve large latent heat exchanges during which temperature remains close to the freeing point. A prolonged pause of the 0°C isotherm at a particular depth gives rise to a condition known as the zero curtain effect. It is noted that the zero curtain temperature is commonly depressed to −0.02°C or to −0.03°C rather than being exactly 0°C due to the presence of solutes in the soil water. Figure 2.6 provides an illustration of such an effect at 1 m depth for a discontinuous permafrost site near Wrigley, NWT (Woo et al. 2006). Ground temperature remained around 0°C for protracted periods both when thawing occurred in May and when freeze-back took place in the autumn.
- Viewed three-dimensionally, soil temperature is affected by vertical and horizontal heat fluxes, which include both the effects of conduction and convection by moisture flow. In view of differential heat flux in vertical and horizontal directions, even adjacent sites can exhibit large differences in active layer freeze-thaw (Carey and Woo 2000).

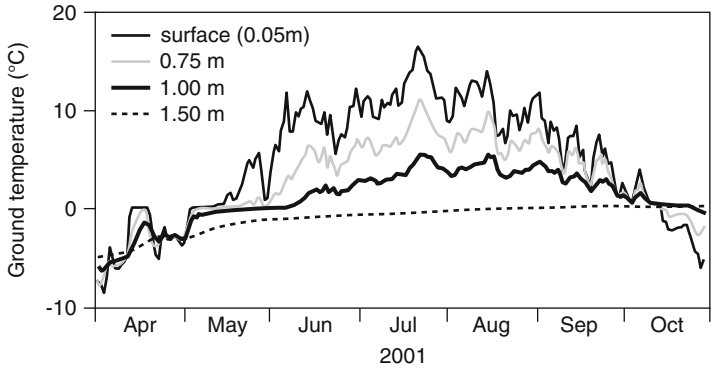

Fig. 2.6 Ground temperature at several depths at a discontinuous permafrost site near Wrigley in central Mackenzie valley. Zero-curtain effects are evident when the ice-rich layer at 1 m depth thawed and froze in 2001 (After Woo et al. 2006)

2.5.1 Penetration of Temperature Waves

As noted above, temperature fluctuations are dampened and lagged as a temperature wave travels down the soil. Analytical solutions are available to describe the descent of periodic waves into isotropic soils that do not experience freeze-thaw. When a temperature wave of amplitude TA_o at the ground surface reaches a depth z, the amplitude TA_z will diminish to

$$TA_z = TA_o \exp[-z\sqrt{\pi/LD_T}] \tag{2.27}$$

The lag time (t_{lag}) for the wave to reach depth z is

$$t_{lag} = 0.5z\,[L/\pi D_T)]^{0.5} \tag{2.28}$$

where D_T is the thermal diffusivity ($m^2\ s^{-1}$) and L is the period (e.g. for a period of 1 day, L = 86,400 s).

The annual temperature wave can be approximated by the first harmonic of a Fourier series (Carson 1963)

$$T_o(t) = \overline{T} + TA_o \sin[2\pi(t + t_{shift})/L] \tag{2.29}$$

with $T_o(t)$ being the surface temperature at time t and t_{shift} being a time shift. Figure 2.7 compares the mean near-surface temperature in the vicinity of Toolik Lake, Alaska (Kane et al. 1991), with estimates using Eq. 2.29. Several reasons cause departures of the fitted curve from the average measured data. (1) A sinusoidal wave may reasonably approximate the annual air temperature cycle, but the effect of this cycle on ground temperature is distorted by the seasonal presence of a

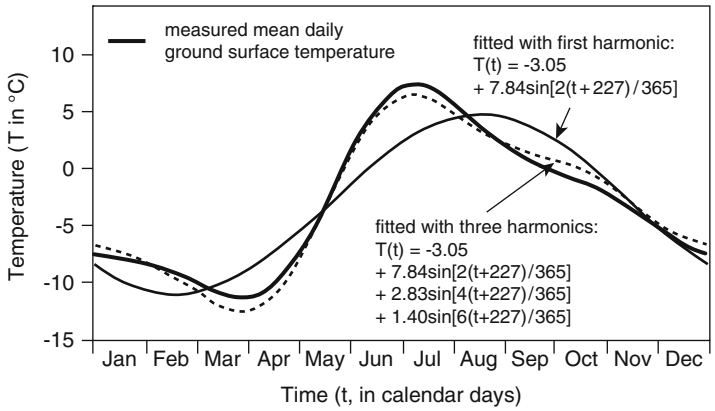

Fig. 2.7 Mean near-surface ground temperature near Toolik Lake, Alaska (From Kane et al. 1991) and curves fitted with first- and third-order harmonics

snow cover. (2) As the solution to a conductive heat equation, the absence of a convective element delays temperature rise in spring when meltwater infiltration raises the ground temperature sooner than is achieved by conduction alone (Kane et al. 1991). (3) Zero-curtain effect due to freeze-thaw of ground ice is not represented in the first harmonic and this is evident in the divergence between the fitted and the measured curves in the freeze-back period. By incorporating higher order harmonics, the Fourier series offers an improved match with the measured data but such an exercise in curve fitting is devoid of physical connotation.

At depth z, the surface temperature wave is dampened and lagged. An analytical solution for the first harmonic is

$$T_z(t) = \overline{T} - (dT/dz)z + TA_z \sin[(2\pi t/L) + z\sqrt{\pi/LD_T}] \tag{2.30}$$

Here, $T_z(t)$ is ground temperature at depth z on day t since the sinusoidal wave begins at the surface,$\overline{T}$is the mean annual surface temperature and dT/dz is the thermal gradient. Note that these analyses do not include freeze-thaw processes, which should be a major consideration in permafrost soils.

The amplitude of the annual temperature wave approaches zero as depth increases. The depth where an annual change of ground temperature is $<0.1°C$ is for practically purposes considered as the depth of zero annual amplitude. Figure 1.6 gives examples of the eventual disappearance of annual temperature variation at depth, based on borehole temperatures obtained by Kristensen et al. (2008) at two sites near Svea in Svalbard. The borehole near the shore gives a depth of about 6–8 m for the zero annual amplitude whereas the zero amplitude depth is deeper at the borehole located 140 m further inland. The shoreline site is warmer in the winter than the inland site, possibly due to the influence of lateral heat exchange with ocean water.

2.5.2 Frost Table Development

Several generalized features pertain to the seasonal development of the active layer (i.e. thawing and freezing leading to deepening or thinning of the seasonally thawed zone).

- The driving force for freeze-thaw is seasonally variable since the energy inputs (Q_G and Q_i) fluctuate according to weather and snow-cover conditions. As the energy supply varies, the rate of active layer development also varies.
- Conduction is the principal mechanism of heat transfer. It is governed by intrinsic thermal properties of the soil layers as well as by drying and wetting and phase changes between water and ice. The insulation property of the moss, lichen and peat that cover extensive areas of the permafrost zone is highly effective in modifying the thermal (and hydrologic) status of the ground (Beringer et al. 2001) and may considerably retard active layer thaw (Yi et al. 2007).
- In ice-rich soils, much heat is consumed in converting water to ice and vice versa. This process gives rise to the zero-curtain effect noted previously and retards the rate of active layer freeze-thaw.
- Surface cooling in early winter shuts off heat supply to the active layer but below the frost table, heat continues to be conducted to the permafrost. This loss of heat cools the bottom of the active layer. When surface temperature drops to the freezing point, descent of the thawing front is halted, but continued heat loss to the permafrost may lead to upward freezing. The active layer is then subject to both down-freezing from the surface and up-freezing from the permafrost table into the thawed active layer. The result is two-sided freezing (Woo et al. 2004). In their case study of active layer freezing on the Alaskan Coastal Plain, Osterkamp and Romanovsky (1997) found that about one-third of the freezing proceeded upward. Moisture can migrate both downward and upward to the freezing fronts, a process that contributes partially to drying at the middle of the active layer. Upward flux of vapor from the frozen soil to the ground surface in winter is another mechanism that desiccates the active layer (Sect. 5.1.3).
- In addition to vertical heat inputs, heat can be conducted and convected laterally. A water body such as a lake or large pond, or a large river and the sea, is a heat source from which heat is conducted to the permafrost zone near the water. Groundwater flow occurs where a hydraulic gradient exists between adjacent sites, and heat is exported with the flow from the higher site to the lower. Both mechanisms can hasten and deepen active layer thaw.
- Thickness of the active layer does vary between years, hence the permafrost table is only approximately constant. In extreme warm years, the active layer thaws deeper than usual and melts away the multi-year ground ice at the top of the former permafrost table. Shur et al. (2005) named this occasionally thawed layer the transition zone. Section 5.3.1.3 further examines summer thaw of the active layer.

2.6 Heat and Moisture Flows in Frozen Soils

Conduction and latent heat exchange are central to heat and moisture flows in the active layer. Several examples are presented to illustrate the spectrum of approaches, with different degree of complexity and level of data demand, hence the potential for application to particular sites or to a broad area.

For a homogeneous soil column that does not undergo freeze-thaw, the difference between the heat that enters the column at depth z and leaves it at depth $z + \Delta z$ is

$$\Delta_{heat} = K_T[(\partial T/\partial z)_z - (\partial T/\partial z)_{z+\Delta z}] \tag{2.31}$$

while the heat gained or lost from this section is

$$\Delta_{heat} = C_T(\partial T/\partial t)\Delta z \tag{2.32}$$

for K_T being the thermal conductivity (W m^{-1} C^{-1}) and C_T the volumetric heat capacity (J m^{-3} C^{-1}) of the soil. Equating these two equations and taking the limit of $\Delta z \rightarrow 0$ yields

$$K_T(\partial^2 T/\partial z^2) = C_T(\partial T/\partial t) \tag{2.33}$$

which is the basic equation for transient heat flow.

Moisture in the active layer is subject to freeze-thaw and Eq. 2.33 is modified to include a latent heat component. The transport of heat and phase change between water and ice in the soil can be stated as

$$\partial[K_T(\partial T/\partial z)]/\partial z = C_T(\partial T/\partial t) - \lambda_f \rho_i(\partial \theta_i/\partial t) \tag{2.34}$$

in which the conducted heat (left-hand side) is used to warm the soil (first term on right hand side of equation) and to freeze the ice (second term). This equation considers that the soil moisture is static and simply freezes or thaws in situ. When moisture flux is taken into consideration, the flow can be written as

$$\partial[K_w(\partial \theta_w/\partial z)(\partial \psi/\partial \theta_w)]/\partial z = \partial \theta_w/\partial t + (\rho_i/\rho_w)(\partial \theta_i/\partial t) \tag{2.35}$$

with the flux of moisture (left hand side of equation) changing the unfrozen water content (first term on right hand side) and altering the amount of ice in the soil (second term on the right). Here, K_T is thermal conductivity (W m^{-1} C^{-1}) and K_w is hydraulic conductivity (m s^{-1}), C_T is volumetric heat capacity of the soil-ice-water-mixture (J m^{-3} C^{-1}), λ_f is latent heat of fusion (J kg^{-1}), ρ_w and ρ_i are the densities of water and ice (kg m^{-3}), T is temperature, t is time, z is depth, θ_w and θ_i are the volumetric fractions of water and ice. ψ is the suction head (m), which changes with the unfrozen water content θ_w, and $\partial \theta_w/\partial z$ indicates the moisture gradient in the soil.

One way to address the coupled heat and moisture flows is to combine Eqs. 2.34 and 2.35 (Guymon et al. 1980; Sheppard et al. 1978) to yield

$$C_{app}(\partial T/\partial t) = \partial[K_{app}(\partial T/\partial z)]/\partial z \tag{2.36}$$

with apparent heat capacity being

$$C_{app} = C_T + \lambda_f \rho_w (\partial \theta_w/\partial T) \tag{2.36a}$$

and apparent thermal conductivity being

$$K_{app} = K_T + \lambda_f \rho_w K_w (\partial \psi/\partial z)(\partial z/\partial T) \tag{2.36b}$$

Finite difference and finite element methods have been used to solve equations such as Eqs. 2.33 or 2.36 (e.g., Jame and Norum 1980; Hromadka et al. 1981), and applied to permafrost soils (Guymon and Luthin 1974; Hinzman et al. 1998, Nakano and Brown 1972). Using these methods to compute temperature change through time (transient temperatures) for a vertical column, the intrinsic thermal properties and initial temperature and moisture contents need to be specified for the soil profile. Standard computation procedure requires upper boundary and lower boundary conditions which are respectively the surface and bottom temperatures during the simulation period. Calculations are performed sequentially at discrete time steps using antecedent temperature and updated thermal properties (C_{app} and K_{app}) obtained from the previous time step for the entire profile, and the boundary conditions for the current time step (Riseborough et al. 2008), until the simulation period ends.

2.6.1 Stefan's Algorithm

A simplified approach, based on Stefan's equation, has been used to calculate ground freeze-thaw in permafrost regions (Carey and Woo 2005; Fox 1992; Woo et al. 2004). The equation was used for the freezing of lake ice and soils by assuming that (1) heat gain or loss is through conduction, (2) sensible heat is negligible and (3) a linear temperature profile in the frozen zone

$$dz_f/dt = K_T(\Delta T_f/\Delta Z_f)/(\lambda_f \rho_w \theta_w) \tag{2.37}$$

where dz_f/dt is the rate of freezing (m s^{-1}), $\Delta T_f/\Delta Z_f$ is the temperature gradient in the frozen zone, K_T is the thermal conductivity of the frozen material (J m^{-1} s^{-1} K^{-1}); λ_f is the latent heat of fusion (J kg^{-1}), ρ_w (kg m^{-3}) and θ_w (m^3/m^3) are density and volumetric content of water. The equation has been adapted using degree-days (DD) to calculate freeze-thaw (Jumikis 1977). The freezing degree-days, for example, is defined as the absolute difference between the daily surface temperature and

the freezing point (usually taken as 0°C) and equals zero when surface temperature is above freezing.

Consider downward freezing of a soil column. Advance of the freezing front is computed using the following procedures.

1. Divide the soil column into a number of slabs (e.g. ten slabs) of thickness ΔZ, and define their thermal conductivities, which also require information on moisture content and minimum unfrozen water content.
2. The thermal resistance of various slabs represents the resistance to the transmission of freezing temperature down the soil column

$$R = Z_f / K_T \tag{2.38}$$

with Z_f and K_T being the thickness and the thermal conductivity of the frozen soil above the frost front, and R having the unit of m^2 s K J^{-1}.
3. When the front reaches slab m, the coldness (H, in degree-days) needed to freeze this slab is

$$H(m) = (\lambda_f \rho_w \theta_w) \Delta z_{un} \left[\sum_{j=1}^{m-1} R(j) + R(m)/2 \right] \tag{2.39}$$

where $0 < \Delta z_{un} < \Delta Z$ is the thickness of the unfrozen zone within slab m.
4. If the degree-day available exceeds the degree-days needed to freeze the slab (i.e. $DD > H$), slab m will be frozen and the frost will penetrate to slab $m + 1$. The remaining degree-days will be available to freeze the lower slab(s) until the residual degree-days are exhausted.
5. If $DD < H$, slab m will only be partially frozen and the freezing depth is

$$\Delta z_f = -K_T(m) \sum_{j=1}^{m-1} R(j) + \left\{ K_T(m)^2 \left[\sum_{j=1}^{m-1} R(j) \right]^2 + \left[\frac{2K_T(m)H(m)}{\lambda_f \rho_w \theta_w} \right] \right\}^{0.5} \tag{2.40}$$

6. The steps are repeated until the freeze-up season is terminated.

The same procedures apply to upward freezing from the permafrost table but the direction is reversed (Woo et al. 2004). To calculate ground thaw, K_T is replaced to represent the thermal conductivity of the thawed material, degree-day becomes the days with temperature above the freezing point and θ_w is substituted by θ_i.

2.6.2 Near-Surface Ground Temperature

Near-surface temperature must be known in order to drive ground temperature computations using numerical models or the Stefan's algorithm but direct temperature measurements are not always available. To estimate the surface temperatures,

various approaches have been formulated, including elaborate techniques that entail surface heat balance (e.g. force-restore method, Deardorff 1977; Li and Koike 2003). Here, only a simple empirical method is described.

The *n*-factor was devised to relate total thawing (or freezing) degree-days of the ground surface to the thawing (or freezing) degree-days in air temperature (Lunardini 1978):

$$n_{thaw} = DD_{thaw}(surface)/DD_{thaw}(air) \tag{2.41}$$

$$DD_{thaw}(air) = \Sigma[T_j(air) - T_b)]$$

and

$$DD_{thaw}(surface) = \Sigma[T_j(surface) - T_b)]$$

with T_j being the mean air or surface temperature on day j, and $T_b = 0°C$ is the freezing temperature. The equivalent for the freezing *n*-factor is a replacement of the thawing- by the freezing degree-days. Riseborough et al. (2008) commented that site-specific *n*-factors are stable between years in continental Arctic, but not so in maritime environments and mountains where there are large interannual variations in the snow cover.

Klene et al. (2001) found that the inclusion of *n*-factor in Stefan's solution considerably improves estimates of active layer thickness. This application applies to total (seasonal) active layer thaw but may not hold for short-term (such as daily) progression of ground freeze-thaw. Woo et al. (2007) found that the ratio of surface to air temperature (T_g/T_a) changes from the beginning to the end of summer at several sites on the Interior Plains in the Mackenzie basin (Fig. 2.8). Three-day running means were used to smooth out fluctuations and based on 5–7 summers of daily measurements, the ratio shows an exponential increase from the beginning of ground thaw (which lags behind the day when mean air temperature rises above 0°C):

$$(T_g/T_a) = b_1 - b_2 \exp(b_3 t) \tag{2.42}$$

where t is the number of days since ground thaw began, b_1, b_2 and b_3 are empirical coefficients. The ratio, which is a function of t, can be used to estimate near surface temperature from the daily air temperature time series.

2.6.3 Moisture Migration and Ice Lens Formation

As the soil cools, advance of the freezing front is accompanied by moisture migration to the front when moisture is available and where the soil texture allows

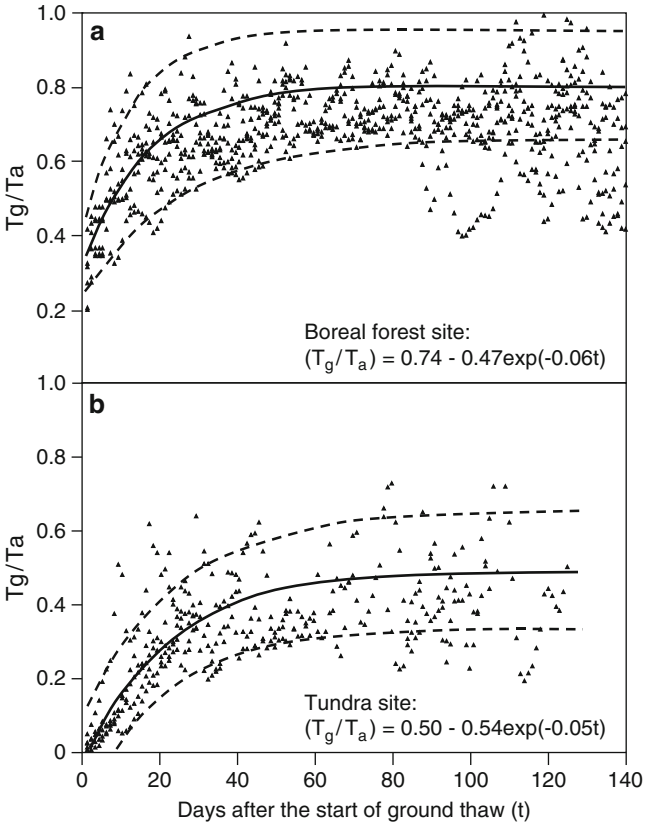

Fig. 2.8 Ratios of ground surface temperature (T_g) and air temperature (T_a) for (**a**) boreal forest and (**b**) tundra sites in the Mackenzie Valley. Three-day running mean temperatures are used to smooth out large daily fluctuations in the measured data. *Full lines* are fitted curves and *dashed lines* are enveloping curves for the data

moisture suction to the front. A soil with such a texture is known as a frost susceptible soil. The processes associated with frost descent, moisture migration and ice formation are summarized as follows.

1. Water that forms the ice may have three origins (Konrad 2001): water within the frozen fringe, water from the unfrozen soil entering the fringe through suction, and for an open system, external water supplied from surrounding areas.
2. Consider the situation of down-freezing in winter. Sudden cooling of the ground (a step change in temperature) leads to rapid descent of the freezing front, freezing the soil water in situ to form pore ice. The ice will increase the soil volume by about 10% of the original unfrozen water content.
3. Below the frost front, there is a coupled flow of heat and moisture. Two mechanisms, termed the capillary and the hydrodynamic models (Smith

1985) have been postulated to account for the resulting formation of segregation ice when water moves from unfrozen soil to the frozen zone.

4. The capillary model hinges on suction created as soil water cools below 0°C.

   - According to the Clausius-Clapeyron relationship, two phases of matter (such as ice and water) can co-exist at a particular temperature

$$dPR/dT = \lambda_f/(T\Delta V) \tag{2.43}$$

   where PR is pressure (Pa, or J m^{-3}), T is temperature (K), λ_f is the latent heat of fusion (=334 kJ kg^{-1}) and ΔV is volume change associated with the phase transition (m^3kg^{-1}). Taking the finite difference form and considering the difference between the pressure on the ice phase (P_i) and the pressure on the water phase (P_w)

$$P_i - P_w = -\lambda_f(T - T_o)/(V_w T_o) \tag{2.44}$$

   Here, T (in K) is the temperature of the water-ice system, T_o is the freezing temperature of pure free water (273.15 K) and V_w is the specific volume of water (0.001 m^3kg^{-1}). The relationship between ($P_i - P_w$) and T (plotted in °C) is shown in Fig. 2.9a (Williams 1986).

   - Small ice crystals in their own melt will have a pressure difference between the solid and the liquid phases. If the ice crystals assume a spherical form with radius r, then the pressure difference is given by (Williams 1967)

$$P_i - P_w = 2\, s_{iw}/r_{iw} \tag{2.45}$$

   with s_{iw} being the surface tension between ice and water (= 0.0305 J m^{-2}), and r_{iw} being the radius of the interfacial curvature.

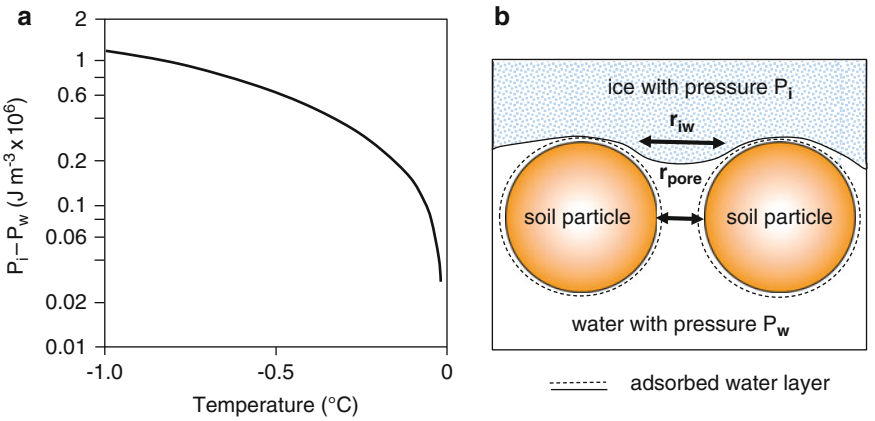

Fig. 2.9 (**a**) Difference between pressure of ice and pressure of water ($P_i - P_w$) increasing as temperature drops (Modified after Williams 1986). (**b**) Capillary model in which ice would penetrate the soil pore if $r_{iw} < r_{pore}$ but the freezing front would halt if $r_{iw} > r_{pore}$

- Equating Eqs. 2.44 and 2.45

$$r_{iw} = -2\, s_{iw} V_w T_o / [\lambda_f (T - T_o)] \tag{2.46}$$

- As temperature drops further below T_o, the denominator in Eq. 2.46 increases and r_{iw} will decrease. Then, two possibilities arise when comparing r_{iw} with the minimum size of soil pores, r_{pore} (Fig. 2.9b):

  (a) If $r_{iw} < r_{pore}$, ice will be able to penetrate the soil pores; ice forms in the pores and the freezing front advances (i.e. descends into the unfrozen zone).

  (b) If $r_{iw} > r_{pore}$, the soil pores are too small for the ice to penetrate and the freezing front is halted.

- With temperature dropping ahead of the freezing front, the pressure of ice (P_i) may remain similar to the atmospheric pressure, but the pressure of water (P_w) will fall below atmospheric, thus creating suction (cryosuction) that brings unfrozen water to the front.
- Under the condition of $r_{iw} > r_{pore}$, continued suction accumulates water at the halted front. As the water freezes, segregated ice is formed and the volumetric increase heaves the soil.

5. The heaving pressure was found to be much underestimated by the capillary model above. An alternative, the hydrodynamic model, considers a hydraulic gradient driven by thermal condition of the soil to send water to the freezing front to form segregated ice.

   - A frozen fringe is envisaged, bounded by the frost front at 0°C (which is the highest temperature at which ice can grow in the soil pore space) and the freezing front where water freezes to form segregated ice lens (Fig. 2.10).
   - The flow of water to the frozen fringe can be calculated using Eq. 2.35. In unfrozen soil, suction is a function of soil moisture content (Clapp and Hornberger 1978) and in frozen soil, it is related to the coexistence of water and ice at temperatures below 0°C. The Clausius-Clapyron relationship (Eq. 2.44) can be applied to provide the requisite suction ($\partial\psi/\partial z$ in Eq. 2.36b):

$$d\psi(T) = -\lambda_f (T - T_o)/(V_w T_o) \tag{2.47}$$

   - Unfrozen water can be transmitted in frozen soil through a thin water film adsorbed to the soil particles because this adsorbed layer remains unfrozen at temperatures much below 0°C.
   - The hydraulic conductivity of frozen soil is reduced drastically as temperature falls. With more unfrozen water entering the frozen fringe than can be transferred, the accumulated water freezes to form ice lens. Smith (1985) suggested that the zone of ice accumulation corresponds with the point at which the temperature drop induces a maximum change in hydraulic conductivity.

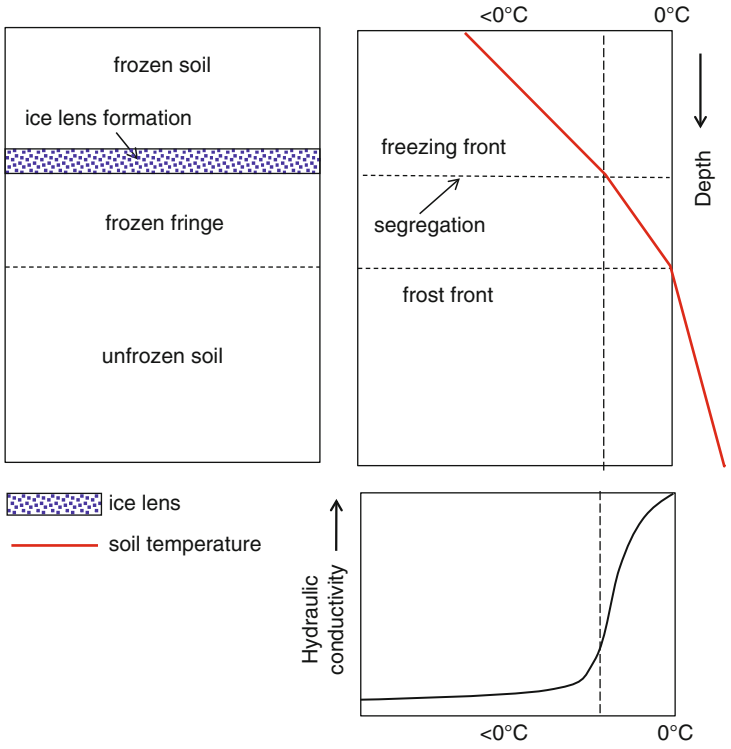

Fig. 2.10 Conceptualization of hydrodynamic and thermal processes that lead to formation of segregated ice; with a frozen fringe bounded by the frost front at 0°C and the freezing front where water freezes to form segregated ice. Water moves upward to the frozen fringe within which hydraulic conductivity drops drastically as temperature falls below 0°C

6. Latent heat generated by segregation ice formation must be dissipated, or the freezing stops.
7. If moisture migration to the freezing front desiccates the unfrozen soil below, suction gradient will diminish and less water will flow to the front. Segregation ceases at this location and the freezing front advances into the unfrozen zone. As the front moves down the soil, condition for ice segregation may again become favorable and the ice lensing process will be repeated.
8. Where an external water source is available, unfrozen water flows continuously to the freezing front when there is a suction gradient. Thus fed, segregated ice can grow to extraordinary thickness.
9. The growth of ice lens at the frost front leads to primary frost heaving. As even frozen soil has some permeability (unfrozen water can move through the interconnected unfrozen water film on the surface of the soil particles), ice can form behind the freezing front. This gives rise to secondary frost heave (O'Neill and Miller 1982) but in this case, ice growth is very slow because of the exceedingly low hydraulic conductivity of the frozen soil.

10. In addition to upward moisture migration to the descending freezing front during active layer freeze-back, moisture moves downward in the summer. As heat is directed downward during the thaw season, moisture migrates from the thawed soil towards the frost table, and ultimately to the permafrost table at the end of the summer.

Frost susceptibility refers to how prone a soil is to frost heaving due to ice segregation. Coarse soils such as gravel and cobbles are not frost susceptible because despite their hydraulic conductivity being high when saturated, the conductivity is very poor at low pore water pressure associated with the freezing front. At the fine-grained extreme, soils such as clay also have poor frost susceptibility because of their very low hydraulic conductivity, which greatly limits the efficiency of water delivery to the freezing front. In between, silty soils are highly frost susceptible as they have good hydraulic conductivity for water transmission and their particle size is small enough that the particles can be ejected by the slowly growing ice crystals (Anderson et al. 1984).

Frost heave is associated with the formation of ground ice which enlarges the soil volume and heaves the ground, mostly upward but also sideways if unconfined. The extent of frost heave depends on

- Soil type: with frost susceptible soils being particularly prone to heaving
- Heterogeneity of soil: in which differential heaving occurs where pockets of frost susceptible soil are mixed with soils of low susceptibility
- Moisture supply: such that under hydrostatic conditions, abundance of free water can freeze and even coarse grained materials can heave considerably.

2.7 Ground Ice

2.7.1 Types of Ground Ice

Water freezing in soil and rock forms ground ice. Ground ice comes from various water sources, freezes through different processes and exhibits a range of forms.

- Pore ice is produced when soil water freezes in situ. Figure 2.11 shows pore ice found in gravels in Resolute. As water freezes, its volume is increased by 10%, but the associated frost heave is minor compared with the growth of segregated ice.
- Segregated ice formation is described in the previous section. Figure 2.12 shows layers of segregated ice in silty soil. Vertical lines of air bubbles in the ice lenses are oriented perpendicular to the downward freezing front. The dilated soil is subject to frost heaving as ice lenses are produced. Segregated ice can grow to tens of meters in thickness (Fig. 2.13).

Fig. 2.11 Pore ice formed in gravels, Resolute

Fig. 2.12 Layers of segregated ice in silty soil, Resolute, with vertical lines of air bubbles in the ice lenses oriented perpendicular to the downward freezing front

Fig. 2.13 Professor Ross Mackay inspecting massive ice exposed on the wall of an ice cellar in Tuktoyaktuk, NWT. Stratification of ice with thin layers of sand suggests segregation origin of ice

Needle ice is a near-surface variant of segregated ice. It can be found at all latitudes and can grow to lengths of several centimeters over a period of several days (Fig. 2.14).

- Vein ice is formed by water freezing in soil cracks and rock fissures and pre-existing ice.

1. Reticulated ice occupies small cracks (formed by thermal contraction or desiccation) to create a three dimensional lattice. They are often found as thin ice veins in fine materials (Fig. 2.15).
2. Foliated ice due to repeated vein-ice formation produces sub-parallel and wavy structure that has air bubbles arranged in the bands. Large contraction cracks in the ground measuring 10^1–10^2 m in length are filled with drifting snow in the winter and with water in summer to form vein ice. Initiation of cracks is attributed to contraction due to low temperatures in the winter. In plan form, the cracks may be perpendicular to each other to constitute an oriented orthogonal (nearly right angle) pattern or they show no preferred orientation but are arranged in a random and often hexagonal fashion (Fig. 2.16a). The frequency of cracking is inversely related to the thickness of snow which provides insulation against the winter coldness. Mackay (1974) found that nearly 40% of the observed wedges cracked each year. Since cracking recurs in the same ice veins, continued infilling of the cracks and freezing create vertically elongated and foliated ice, tapering downward to form a wedge-shaped cross section (Fig. 2.16b). Ice wedges are usually <1 m wide at the top, and reach 3–4 m or even wider across in Siberia.

Fig. 2.14 Needle ice on a high altitude hillslope of Haleakala National Park, Maui Island, Hawaii

Fig. 2.15 Reticulated vein ice in frozen clay beneath a wetland in Resolute. Note frost crystals in the top moss layer formed by condensation of vapor that fluxed upward from the soil

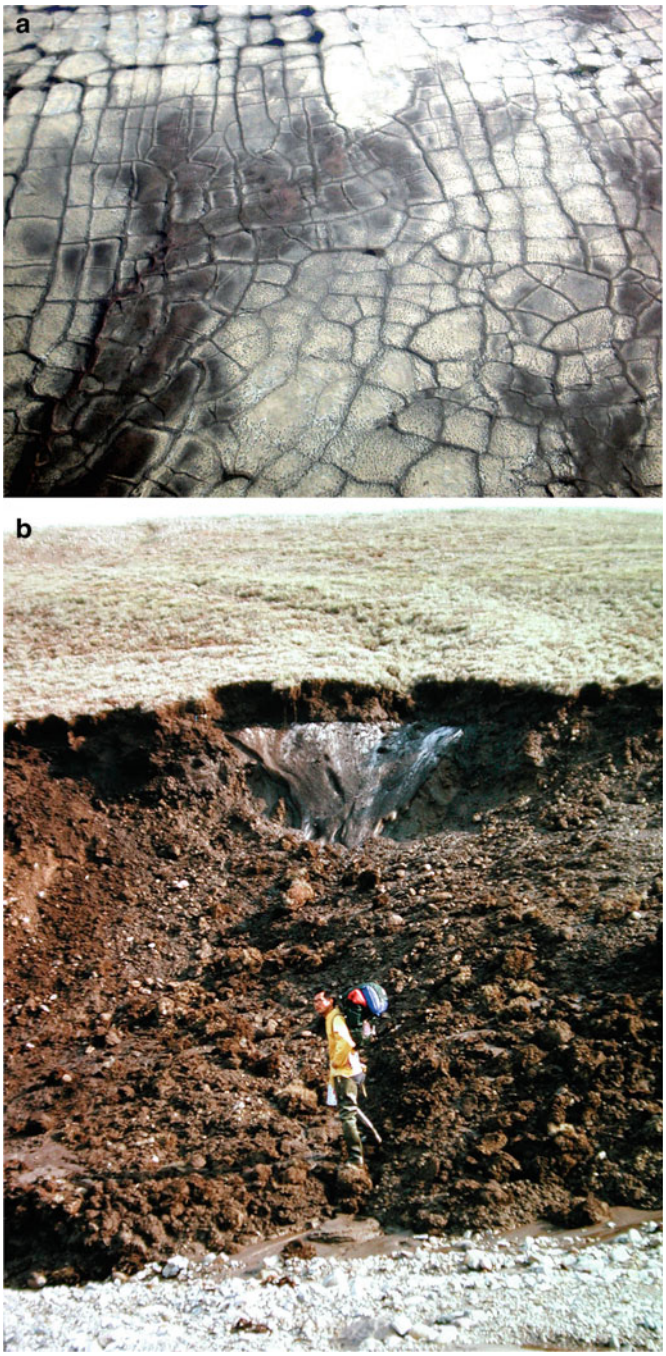

Fig. 2.16 (**a**) Ice-wedge polygons near Eureka, Ellesmere Island. Most polygons show oriented orthogonal patterns except those at the lower right corner which exhibit outlines without preferred orientations. (**b**) Slumping exposing the cross section of an ice wedge that underlies a polygonal crack, Vendom Fiord, Ellesmere Island

Fig. 2.17 Seasonal frost mound near Sinuk, Alaska, underlain by intrusive ice formed by freezing of groundwater injected under the surface peat and clay layer

- Intrusive ice is formed by water injected into ice or frozen materials under pressure. It can be seasonal or perennial ice. Figure 2.17 shows intrusive ice that lifts a seasonal frost mound near Sinuk, Alaska. Water injected under hydrostatic or hydraulic pressures constitutes pingo ice when frozen. The mechanisms are described in Sect. 3.5.
- Other ice types encompass all the ground ice that does not fall under the above categories. They vary from pool ice, such as ice that forms in a pool resting atop an ice wedge (Fig. 2.18), to cavity ice, which is hoar frost that grows in underground space (Fig. 2.19).
- Massive ice is a general term that refers to a large ground ice body (Fig. 2.20). It usually consists of various types of ice that can include segregated, intrusive and vein ice, as well as buried surface ice which could have been snow or glacier ice, lake, sea and river ice.

2.7.2 Excess Ice

Excess ice is the volume of ice-melt water that exceeds the pore space available in the host material under natural unfrozen conditions (Fig. 2.21). Thawing of soils with large quantities of ground ice yields considerable amounts of liquid water, enabling augmentation of moisture elsewhere in the soil profile and replenishment of groundwater. The soil gradually consolidates under its own weight. If, however, thawing releases water more rapidly than can be drained, a positive pressure will develop within the interstitial water. With water carrying part of the weight of the

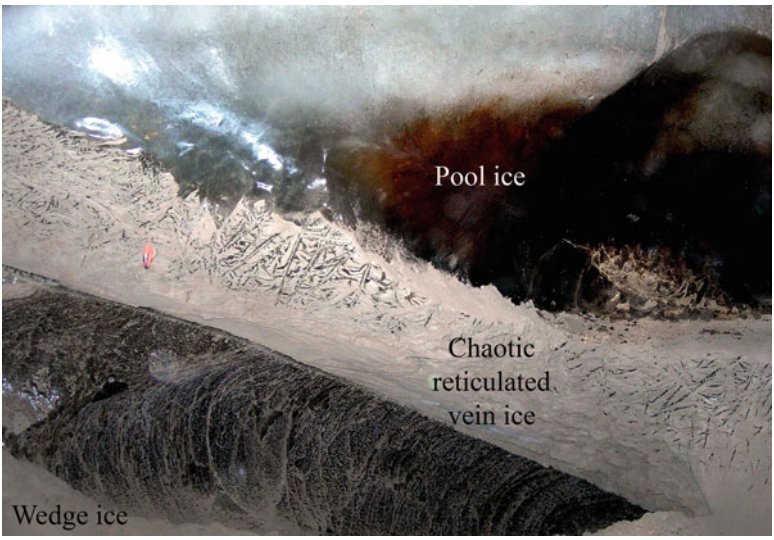

Fig. 2.18 Pool ice above a silt layer with chaotic reticulated vein ice that rests on wedge ice, Permafrost Tunnel, Fairbanks, Alaska. Pool ice has brownish tint due to organic content; chaotic pattern of reticulated vein ice was produced as soil water froze in any available cracks when squeezed between the descending freezing front and the permafrost; wedge ice beneath shows distinct foliated fabric

Fig. 2.19 Hoar frost, considered as cavity ice, attached to the ceiling of an ice cellar in Tuktoyaktuk

Fig. 2.20 Massive ice in Arctic, Antarctic and high plateau locations: (**a**) exposed on a gully wall and along coastal bluff near Tuktoyaktuk, NWT, (**b**) formed of glacier ice buried by materials erupted from a volcano at Telefon Bay, Deception Island, and (**c**) revealed beneath a reddish silty-clay layer along the wall of a thermokarst depression, Tibetan Highway at Erdaugou

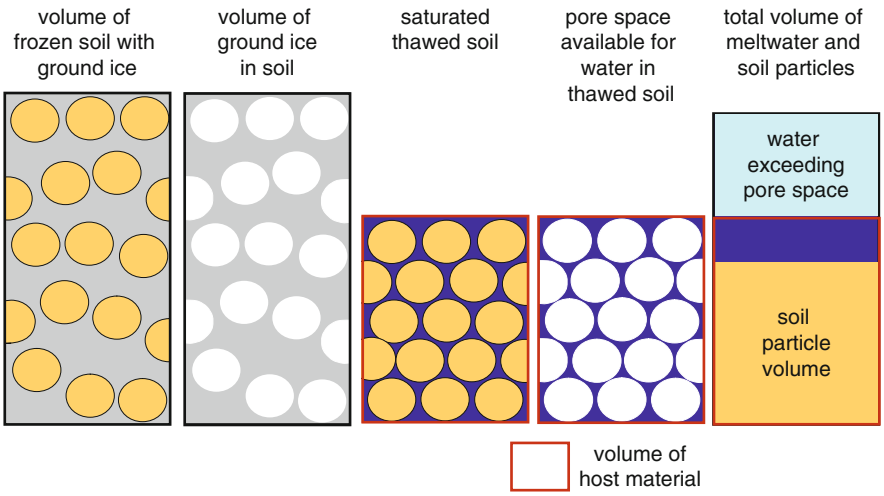

Fig. 2.21 Conceptualization of excess ice in frozen soil which upon thawing and soil consolidation, offers insufficient space to hold all the ice-melt water. The extra volume that cannot be retained in the thawed host material is known as excess ice

Fig. 2.22 A track at the left and a temporary runway on the tundra lead to a cluster of thermokarst ponds. Thermokarst process has also enlarged the cracks of several ice-wedge polygons, Fosheim Peninsula, Ellesmere Island

overburden, a 'quick' condition follows. The soil mass loses strength and behaves like a viscous liquid (McRoberts and Morgenstern 1974).

Draining of icemelt water can produce surface runoff while the accompanying loss of volume leads to ground subsidence and slope failure. These processes are

central to thermokarst development. Thermokarst produces linear troughs, irregular depressions with pools, ponds and thawed lakes (Fig. 2.22). Erosion by running water further modifies and enlarges these features. In some situations, surface erosion and slumping degrade the topography to badland-like landscapes.

References

Anderson DM, Williams PJ, Guymon GL, Kane DL (1984) Principles of soil freezing and frost heaving. In: Berg RL, Wright EA (eds) Frost action and its control. American Society of Civil Engineers, New York, pp 1–21

Barry RB, Hare FK (1974) Arctic climate. In: Ives JD, Barry RG (eds) Arctic and alpine environments. Methuen, London, pp 17–54

Bello R, Smith JD (1990) The effect of weather variability on the energy balance of a lake in the Hudson Bay Lowlands, Canada. Arctic Alpine Res 22:98–107

Benson CS (1970) Ice fog. Low temperature air pollution defined with Fairbanks, Alaska as type locality. US Army CRREL research report 121

Beringer J, Lynch AH, Chapin FS III, Mack M, Bonan GB (2001) The representation of Arctic soils in the land surface model: the importance of mosses. J Clim 14:3324–3335

Boike J, Wille C, Abnizova A (2008) Climatology and summer energy and water balance of polygonal tundra in the Lena River Delta, Siberia. J Geophys Res 113:G03025. doi:10.1029/2007JG000540

Bovis MJ, Barry RG (1974) A climatological analysis of north polar desert areas. In: Smiley TL, Zumberge JH (eds) Polar deserts and modern man. University of Arizona Press, Tuscon, pp 23–31

Brown J, Dingman SL, Lewellen RI (1968) Hydrology of a drainage basin on the Alaska coastal plain. US Army CRREL special report 24C

Bryson RA (1966) Air masses, streamlines and the boreal forest. Geogr Bull 8:228–269

Carey SK, Woo MK (2000) Within slope variability of ground heat flux, subarctic Yukon. Phys Geogr 21:407–417

Carey S, Woo MK (2005) Freezing of subarctic hillslopes, Wolf Creek Basin, Yukon, Canada. Arct Antarct Alp Res 37:1–20

Carson JE (1963) Analysis of soil and air temperatures by Fourier techniques. J Geophys Res 68:1070–1078

Clapp RB, Hornberger GM (1978) Empirical equations for some soil hydraulic properties. Water Resour Res 14:601–604

Connolley WM, Cattle H (1994) The Antarctic climate of the UKMO unified model. Antarct Sci 6:115–122

Davies JA (1972) Actual, potential and equilibrium evaporation for a beanfield in southern Ontario. Agr Meteorol 10:331–348

Deardorff JW (1977) Efficient prediction of ground surface temperature and moisture with inclusion of a layer of vegetation. J Geophys Res (Atmos) 83:1889–1903

Derksen C, Brown R, MacKay M (2008) Mackenzie Basin snow cover: variability and trends from conventional data, satellite remote sensing, and Canadian regional climate model simulations. In: Woo MK (ed) Cold region atmospheric and hydrologic studies, the Mackenzie GEWEX experience, vol 1, Atmospheric dynamics. Springer, Berlin, pp 213–239

de Vries DA (1963) Theoretical properties of soils. In: van Wijk WR (ed) Physics of plant environment. North-Holland, Amsterdam, pp 210–235

Dilley AC (1968) On the computer calculation of vapor pressure and specific humidity gradients from psychrometric data. J Appl Meteorol 7:717–719

Farouki OT (1981) The thermal properties of soils in cold regions. Cold Reg Sci Technol 5:67–75

Fox JD (1992) Incorporating freeze-thaw calculations into a water balance model. Water Resour Res 28:2229–2244
Guymon GL, Hromadka TV II, Berg RL (1980) A one dimensional frost heave model based upon simulation of simultaneous heat and water flux. Cold Reg Sci Technol 3:253–262
Guymon GL, Luthin JN (1974) A coupled heat and moisture transport model for Arctic soils. Water Resour Res 10:995–1001
Hinzman LD, Goering DJ, Kane DL (1998) A distributed thermal model for calculating soil temperature profiles and depth of thaw in permafrost regions. J Geophys Res 103 (D22):28,975–28,991
Hinzman LD, Kane DL, Gieck RE, Everett KR (1991) Hydrologic and thermal properties in the active layer in the Alaskan Arctic. Cold Reg Sci Technol 19:95–110
Hoskins BJ, Hodges KI (2005) A new perspective on southern hemisphere storm tracks. J Clim 18:4108–4129
Hromadka TV II, Guymon GL, Berg RL (1981) Some approaches to modeling phase change in freezing soils. Cold Reg Sci Technol 4:137–145
Hudak DR, Young JMC (2002) Summer climatology of the southern Beaufort Sea. Atmos Ocean 40:145–158
Jame YW, Norum DI (1980) Heat and mass transfer in a freezing unsaturated porous medium. Water Resour Res 16:811–819
Jumikis AR (1977) Thermal geotechnics. Rutgers University Press, New Brunswick
Kane DL, Hinzman LD, Zarling JP (1991) Thermal response of the active layer to climatic warming in a permafrost environment. Cold Reg Sci Technol 19:111–122
Klene AE, Nelson FE, Shiklomanov NI, Hinkel KM (2001) The n-factor in natural landscapes: variability of air and soil-surface temperatures, Kuparuk River Basin, Alaska, U.S.A. Arct Antarct Alp Res 33:140–148
Konrad J-M (2001) Cold region engineering. In: Rowe RK (ed) Geotechnical and geoenvironmental engineering handbook. Kluwer, Dordrecht, pp 593–613
Kristensen L, Christiansen HH, Caline F (2008) Temperature in coastal permafrost in the Svea area, Svalbard. In: Proceedings of the 9th international conference on permafrost., Fairbanks, Alaska. University of Alaska, Fairbanks, pp 1005–1010
Li X, Koike T (2003) Frozen soil parameterization in SiB2 and its validation with GAME-Tibet observations. Cold Reg Sci Technol 36:165–182
Lunardini VJ (1978) Theory of n-factors and correlation of data. In: Proceedings of the 3rd international conference on permafrost, vol 1. National Research Council of Canada, Ottawa, pp 40–46
Mackay JR (1974) Ice wedge cracks, Garry Island, Northwest Territories. Can J Earth Sci 11:1366–1383
Marsh P, Bigras SC (1988) Evaporation from Mackenzie delta lakes, N.W.T., Canada. Arctic Alpine Res 20:220–229
Marsh P, Rouse WR, Woo MK (1981) Evaporation at a high Arctic site. J Appl Meteorol 20:713–716
McRoberts EC, Morgenstern NR (1974) The stability of thawing slopes. Can Geotech J 11:447–469
Mendez J, Hinzman LD, Kane DL (1998) Evapotranspiration from a wetland complex on the Arctic coastal plain of Alaska. Nord Hydrol 29:303–330
Nakano Y, Brown J (1972) Mathematical modeling and validation of the thermal regimes in tundra soils, Barrow, Alaska. Arctic Alpine Res 4:19–38
Nicholson FH (1976) Permafrost thermal amelioration tests near Schefferville, Quebec. Can J Earth Sci 13:1694–1705
Ohmura A (1982) Objective criteria for rejecting data for Bowen ratio flux calculations. J Appl Meteorol 21:595–598
Oke TR (1987) Boundary layer climates, 2nd edn. Routledge, London

O'Neill K, Miller RD (1982) Numerical solutions for a rigid-ice model of secondary frost heave. US Army CRREL Report 82–13
Osterkamp TE, Romanovsky VE (1997) Freezing of the active layer on the coastal plain of the Alaskan Arctic. Permafrost Periglac 8:23–44
Priestley CHB, Taylor RJ (1972) On the assessment of surface heat flux and evaporation using large-scale parameters. Mon Weather Rev 100:81–92
Riseborough D, Shiklomonov N, Etzelmüller B, Gruber S, Marchenko S (2008) Recent advances in permafrost modeling. Permafrost Periglac 19:137–156
Rouse WR, Mills PF, Stewart RB (1977) Evaporation in high latitudes. Water Resour Res 13:909–914
Serreze MC, Barry RG (2005) The Arctic climate system. Cambridge University Press, Cambridge
Sheppard MI, Kay BD, Loch JPG (1978) Development and testing of a computer model for heat and mass flow in freezing soils. In: Proceedings of the 3rd international conference on permafrost, Edmonton, Alberta, vol 1. National Research Council of Canada, Edmonton, pp 75–81
Shur Y, Hinkel KM, Nelson FE (2005) The transient layer: implications for geocryology and climate-change science. Permafrost Periglac 16:5–17
Shutov V, Gieck RE, Hinzman LD, Kane DL (2006) Evaporation from land surface in high latitude areas: a review of methods and study results. Nord Hydrol 37:393–411
Simmonds I, Keay K, Lim EP (2003) Synoptic activity in the seas around Antarctica. Mon Weather Rev 131:272–288
Smith MW (1985) Models of soil freezing. In: Church MA, Slaymaker HO (eds) Field and theory: lectures in geocryology. University of British Columbia Press, Vancouver, pp 96–120
Stewart RB, Rouse WR (1977) Substantiation of the Priestley and Taylor parameter α-1.26 for potential evaporation in high latitudes. J Appl Meteorol 16:649–650
Szeto KK, Liu JL, Wong A (2008a) Precipitation recycling in the Mackenzie and three other major river basins. In: Woo MK (ed) Cold region atmospheric and hydrologic studies, the Mackenzie GEWEX experience, vol 1, Atmospheric dynamics. Springer, Berlin, pp 137–154
Szeto KK, Stewart RE, Yau MK, Gyakum J (2008b) The Mackenzie climate system: a synthesis of MAGS atmospheric research. In: Woo MK (ed) Cold region atmospheric and hydrologic studies, the Mackenzie GEWEX experience, vol 1, Atmospheric dynamics. Springer, Berlin, pp 23–50
Williams PJ (1967) The nature of freezing soil and its field behavior. Norwegian Geotech Inst Publ 72:91–119
Williams PJ (1986) Pipelines and permafrost: science in a cold climate. Carleton University Press, Ottawa
Woo MK, Arain A, Mollinga M, Yi S (2004) A two-directional freeze and thaw algorithm for hydrologic and land surface modelling. Geophys Res Lett 31:L12501. doi:10.1029/2004GL019475
Woo MK, Mollinga M, Smith SL (2006) Simulating active layer thaw in a boreal environment. Geogr Phys Quatern 60:9–17
Woo MK, Mollinga M, Smith SL (2007) Climate warming and active layer thaw in the boreal and tundra environments of the Mackenzie Valley. Can J Earth Sci 44:733–743
Woo MK, Steer P (1979) Measurement of trace rainfall at a high Arctic site. Arctic 32:80–84
Yi S, Woo MK, Arain A (2007) Impacts of peat and vegetation on permafrost degradation under climate warming. Geophys Res Lett 34:L16504. doi:10.1029/2007GL030550
Zhou YW, Guo DX, Qiu GQ, Cheng GD, Li SD (2000) Geocryology in China. Chinese Academy of Sciences, Beijing

http://www.springer.com/978-3-642-23461-3

Permafrost Hydrology
Woo, M.-k.
2012, XII, 564 p., Hardcover
ISBN: 978-3-642-23461-3